

Density-of-states effective mass and scattering parameter measurements by transport phenomena in thin films

D. L. Young, T. J. Coutts, and V. I. Kaydanov

Citation: [Review of Scientific Instruments](#) **71**, 462 (2000); doi: 10.1063/1.1150224

View online: <http://dx.doi.org/10.1063/1.1150224>

View Table of Contents: <http://scitation.aip.org/content/aip/journal/rsi/71/2?ver=pdfcov>

Published by the [AIP Publishing](#)

Articles you may be interested in

[Electron transport and band structure in phosphorus-doped polycrystalline silicon films](#)

J. Appl. Phys. **105**, 033715 (2009); 10.1063/1.3068349

[Nitrogen-induced decrease of the electron effective mass in GaAs \$1-x\$ N \$x\$ thin films measured by thermomagnetic transport phenomena](#)

Appl. Phys. Lett. **82**, 1236 (2003); 10.1063/1.1554777

[Growth and characterization of radio frequency magnetron sputter-deposited zinc stannate, \$\text{Zn}_2\text{SnO}_4\$, thin films](#)

J. Appl. Phys. **92**, 310 (2002); 10.1063/1.1483104


[Direct measurement of density-of-states effective mass and scattering parameter in transparent conducting oxides using second-order transport phenomena](#)

J. Vac. Sci. Technol. A **18**, 2978 (2000); 10.1116/1.1290372


[Electronic transport in tin-doped indium oxide thin films prepared by sol-gel technique](#)

J. Appl. Phys. **83**, 2139 (1998); 10.1063/1.366949


Frustrated by old technology?



Is your AFM dead and can't be repaired?



Sick of bad customer support?




It is time to upgrade your AFM

Minimum \$20,000 trade-in discount for purchases before August 31st

Asylum Research is today's technology leader in AFM

dropmyoldAFM@oxinst.com



Density-of-states effective mass and scattering parameter measurements by transport phenomena in thin films

D. L. Young and T. J. Coutts

National Renewable Energy Laboratory, 1617 Cole Boulevard, Golden, Colorado 80401

V. I. Kaydanov^{a)}

Colorado School of Mines, Golden, Colorado 80401

(Received 31 August 1999; accepted for publication 27 September 1999)

A novel machine has been developed to measure transport coefficients in the temperature range of 50–350 K of thin films deposited on electrically insulating substrates. The measured coefficients—resistivity, Hall, Seebeck, and Nernst—are applied to solutions of the Boltzmann transport equation to give information about the film's density-of-states effective mass, the Fermi energy level, and an energy-dependent scattering parameter. The machine is designed to eliminate or compensate for simultaneously occurring transport phenomena that would interfere with the desired measured quantity, while allowing for all four coefficients to be measured on the same sample. An average density-of-states effective mass value of $0.29 \pm 0.04 m_e$ was measured on the transparent conductive oxide, cadmium stannate (CTO), over a carrier concentration range of $2\text{--}7 \times 10^{20} \text{ cm}^{-3}$. This effective mass value matched previous results obtained by optical and thermoelectric modeling. The measured scattering parameter indicates that neutral impurities or a mixture of scattering mechanisms may inhibit the transport of carriers in CTO. © 2000 American Institute of Physics. [S0034-6748(00)02802-1]

I. INTRODUCTION

Characterization of materials by measurement of carrier transport properties offers valuable insight into their physical character. Some of the more common transport phenomena are resistivity, Hall, and Seebeck effects; other lesser-known phenomena include Nernst, Ettingshausen, and Righi–Leduc effects. Early experiments on transport phenomena were performed on bulk, single-crystal samples^{1–4} and provided information on carrier degeneracy and type, scattering mechanisms, Fermi level, effective mass, and band structure.^{5,6} Currently, a resurgence of characterization of materials by transport phenomena is occurring in the thin-film community.^{7–9}

Transparent conductive oxide (CTO) thin films are finding their place in large-volume applications, yet they remain some of the least-understood semiconducting materials. One reason for this is that CTOs and other thin films often suffer from relatively poor transport properties. Traditional experimental methods for probing the Fermi surface, such as measuring effective mass using de Haas–van Alphen and other resonance techniques, require samples to have large mobilities and long relaxation times. CTOs, with their low mobilities ($< 200 \text{ cm}^2/\text{V s}$) and short relaxation times ($\sim 10^{-15} \text{ s}$), are excluded from these techniques. Zhitinskaya *et al.*¹⁰ developed a method, based on earlier work by Kolodziejczak, Zukotynski, and Zawadzki,^{11,12} that uses solutions to the Boltzmann equation by which the measured value of four transport coefficients (resistivity, Hall, Seebeck, and Nernst) can reveal the Fermi energy level, the density-of-states effective

mass, and an energy-dependent scattering parameter related to a relaxation time. These four transport coefficients can be measured on a thin-film sample if proper care is taken to eliminate or compensate for competing transport phenomena. We have developed a method and an instrument to measure resistivity, Hall, Seebeck, and transverse Nernst coefficients on a thin film deposited on an electrically insulating substrate. These coefficients can be measured over the temperature range of 50–350 K, thereby providing further insights on the transport phenomena.

II. SAMPLE CONFIGURATION

CTOs and other thin films are deposited on electrically insulating substrates (Corning 7059) and then patterned using standard photolithographic techniques. The shape of the pattern is shown in Fig. 1. The pattern has four contact pads, marked 1–4, with $a \ll W$, $b \ll L$, and $W < L$. The first two dimensions provide small-area contacts critical for the van der Pauw technique, whereas the latter dimension ensures a large transverse Nernst signal by maximizing the temperature gradient between contacts 2 and 4 and the Nernst voltage between contacts 1 and 3. This pattern conforms to the specimen shape specified in the ASTM designation F 76–86¹³ for van der Pauw resistivity and Hall measurements. The thickness of the film is measured by either stylus profilometry or ellipsometry. Samples are mounted film-side down across heater blocks A and B, as shown in Fig. 2(a). Good electrical and thermal contact to the heater blocks is made to contact pads 2 and 4 with silver paint, followed by an anneal under a hot lamp. A small amount of thermal grease is placed between the substrate and the heater blocks to improve thermal contact and temperature uniformity along

^{a)}Formerly Kaidanov.

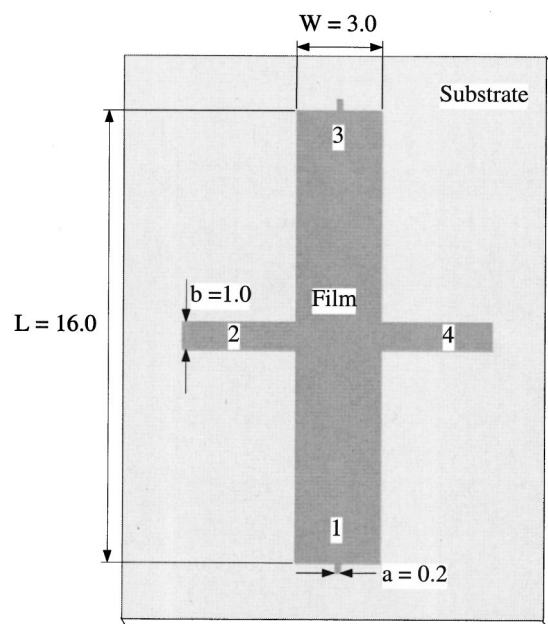


FIG. 1. Patterned thin film on electrically insulating substrate. Dimensions are in mm.

the sample's length. Contact pads 1 and 3 are indium-soldered to copper wire 0.0076 cm (0.003 in.) in diameter, which minimizes conductive heat loss from the sample through contacts 1 and 3.

III. DEVICE DESCRIPTION

The sample holder, shown in Figs. 2(a) and 2(b), is made from OFHC copper and is thermally attached to an Air Products DE 202S closed-cycle helium two-stage cryostat. Copper heater blocks A and B are electrically isolated from the sample-holder stage and each other, but thermally connected via a sheet of 0.238 cm (3/32 in.) grade G-10 Garolite™. The heating elements in the heater blocks are carbon resistors mounted with Stycast™ epoxy in holes bored through the center of the heating blocks parallel to their long axis. Embedded in, but electrically isolated from, the heater blocks is a type E differential thermocouple made from 0.013 cm (0.005 in.) diameter wire, depicted in Fig. 2(b). The joints of the differential thermocouple are located as close as possible to the mounting surface of the heater blocks and are thermally anchored with Stycast™ epoxy. Heater block B also has an electrically isolated type E thermocouple mounted adjacent to one of the differential thermocouple junctions, and it too is secured with epoxy. All the thermocouple junctions are located just under the surface of the copper blocks, exactly where the sample mounting tabs 2 and 4 are located. Both heater blocks are drilled and tapped with 4–40 holes on the inside of the channel between the blocks. Thermocouple-grade, solid copper wire 0.025 cm (0.010 in.) in diameter is crimped to a copper spade lug and attached to the copper block with a 4–40 screw. Care was taken to remove any residual copper oxide, because of its relatively large Seebeck coefficient, using reliable methods.¹⁴ All of the wires exiting the sample holder are wound in twisted pairs to minimize magnetic interference, and these pairs are wound around the

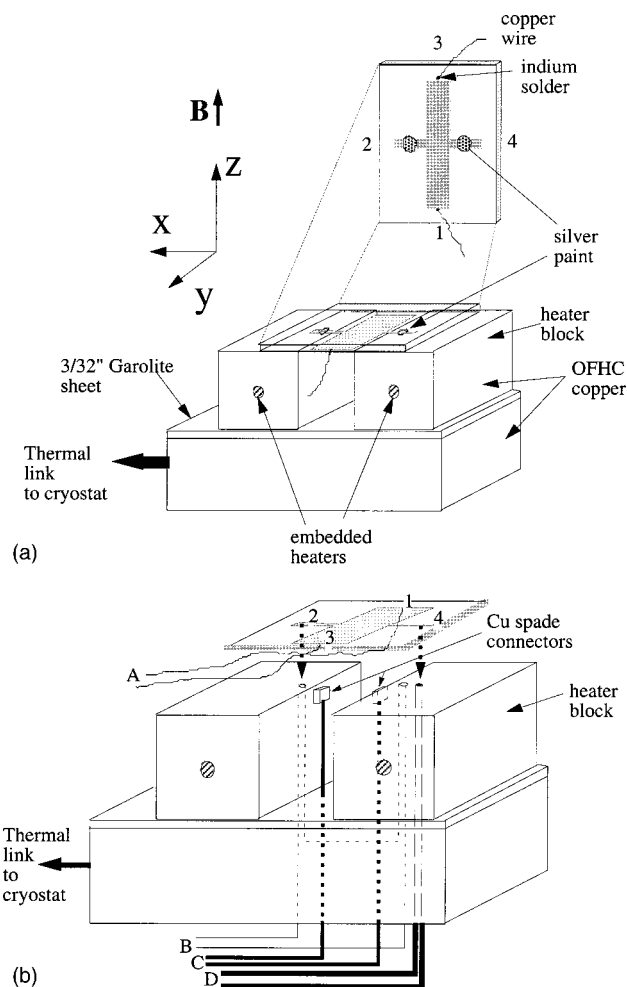


FIG. 2. (a) Schematic of sample holder with sample mounted film-side down across the heater blocks. Not shown are two small clamps used to press the sample against the heater blocks. (b) View of sample holder showing thermocouple and contact lead placement. (A) Cu leads for contacts 1, 3; (B) type E differential thermocouple; (C) Cu leads for contacts 2, 4; (D) type E thermocouple. Thermocouples B and D are located just under the surface of the heater blocks directly below sample contacts 2, 4.

cryostat expander arm multiple times to minimize heat conduction. These wires are connected to a nanovolt-meter card and a multiplexer card within a Keithley 7001 scanner after passing through an isothermal, thermocouple-grade barrier strip inside the cryostat. The scanner is attached to a Keithley 182 nanovolt meter and two Keithley 220 current sources—one for controlling the carbon resistor heaters and the other for biasing the sample. All of the instruments are computer controlled via a GPIB 488.2 line and automated by a custom LabView™ program. A schematic of the system is shown in Fig. 3.

IV. DATA COLLECTION SEQUENCE

Patterned samples are mounted film-side down on the sample holder, and contacts are checked to ensure ohmicity by plotting current vs. voltage. Next, a stainless-steel shroud is placed over the cryohead, evacuated to 40 mTorr, and lowered between the poles of an electromagnet capable of producing a magnetic field of up to 0.6 T. With both heater blocks at the same temperature, measurements of the van der

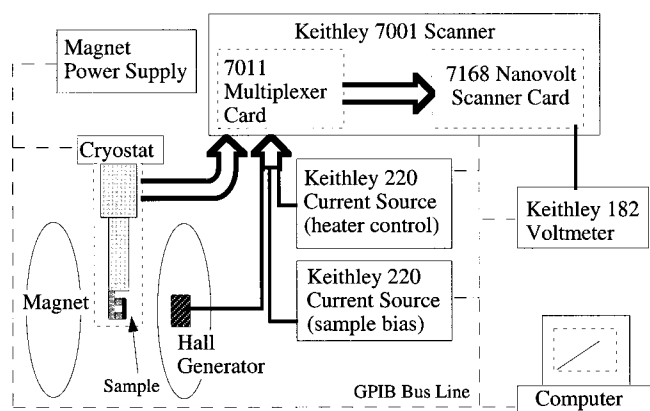


FIG. 3. Schematic of instrumentation associated with the transport phenomena instrument.

Pauw resistivity begin by first zeroing the offset voltages due to stray thermovoltages in the system. Next, contacts 1 and 2 are biased, while the van der Pauw voltage is measured between contacts 3 and 4. This sequence is repeated for reversed current and for the remaining three configurations of contact pairs, as per ASTM designation F 76–86.

The Hall coefficient is measured by first turning on the magnetic field perpendicular to the sample plane [Fig. 2(a)]. The induction and direction of the magnetic field are measured by a Hall generator mounted between the poles of the magnet. After a reasonable amount of settling time for the field, contacts 1 and 3 are biased, and the Hall voltage is measured between contacts 2 and 4. Again, this sequence is repeated for reversed current and reversed magnetic field for the remaining configuration of contact pairs, as per ASTM designation F 76–86. Thermal and contact misalignment offset voltages are zeroed, while maintaining isothermal conditions in the sample minimizes errors due to the Ettingshausen effect. Recall that the Ettingshausen effect is a temperature gradient that arises in a magnetic field due to the thermal distribution in the electron velocities. For instance, if electrons flow from contacts 4 to 2 [Fig. 4(a)] with a z -directed magnetic field, the magnetic field will divert the “hot” (fast) electrons less than the “cold” (slow) electrons.¹⁵ This con-

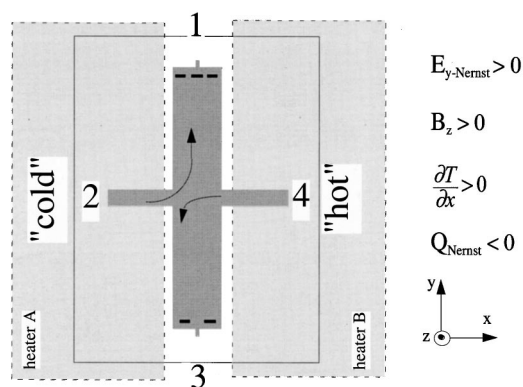


FIG. 4. Transverse Nernst effect. Arrows indicate direction of flow for diffusing electrons deflected by the magnetic field for a material with a negative Nernst coefficient. The less energetic, “cold” electrons from contact 2 are deflected more by the magnetic field, giving rise to a net negative charge at contact 1.

dition establishes a temperature gradient directed from contact 3 to 1. The temperature gradient will then generate a Seebeck electric field from contact 1 to 3 (n -type materials). Note that this Ettingshausen induced field is superimposed on the Hall field and cannot be subtracted by either reversal of the current or the magnetic field. Thus, isothermal conditions must be maintained within the sample to counteract the Ettingshausen effect. Fortunately, the relatively thick substrate acts as a large thermal mass for the film and hence maintains good isothermal conditions across the film. Similarly, this same substrate thermal mass also acts to decrease the magnitude of the Peltier effect during both the resistivity and the Hall measurements.

Thermoelectric and thermomagnetic effects are measured with a temperature gradient $\nabla_x T$ across the film by turning on one of the heaters. For the Seebeck coefficient, we turn off the magnetic field and measure the temperature difference between the heater blocks ($\Delta T_{2,4}$) with the differential thermocouple and the voltage difference ($\Delta V_{2,4}$) between contacts 2 and 4. The Seebeck coefficient can be approximated by $\alpha = \Delta V_{2,4} / (\Delta T_{2,4})$. To eliminate offset voltage errors, $\Delta V_{2,4}$ is measured for several values of $\Delta T_{2,4}$, and the slope of the best-fit line of $\Delta V_{2,4}$ versus $\Delta T_{2,4}$ gives the Seebeck coefficient of the film and the sample-holder couple for a film temperature equal to the average temperature of blocks A and B. To eliminate the Seebeck contribution from the sample holder, a calibration curve was made with 99.96% pure Pb and verified by 99.998% pure Pt, which both have known values of absolute Seebeck coefficients over a wide range of temperatures.^{16,17} The Seebeck coefficient of the sample holder was found, not surprisingly, to be very close to that of copper. This value is added to the measured Seebeck value to obtain the absolute Seebeck coefficient for the film.

The Nernst coefficient is measured by turning on the magnetic field perpendicular to the plane of the film while maintaining the temperature gradient $\partial T / \partial x$ across the film. The magnetic field and the temperature gradient establish an isothermal, transverse Nernst voltage between contacts 1 and 3. The Nernst field is analogous to the Hall field, except that the charge carriers move due to a temperature gradient, rather than by an applied bias. The isothermal, transverse Nernst coefficient, Q , can be measured according to

$$E_y = -Q \frac{\partial T}{\partial x} B_z.$$

Figure 4 depicts the generation of a Nernst voltage for a material with a negative Nernst coefficient. By reversing the magnetic field, remeasuring the Nernst voltage, and averaging the difference of the two values, we eliminate offset thermoelectric voltages in the system. Because Nernst voltages tend to be in the nanovolt range, it is advantageous to measure the Nernst coefficient by extracting the slope from plots of $\Delta V_{1,3}$ vs $\Delta T_{2,4}$ or $\Delta V_{1,3}$ vs B_z . As mentioned earlier, our system is cooled by a closed-cycle helium cryostat that transfers some vibration to the sample. These vibrations may cause stray voltages to develop in our sample wires when the magnetic field is on and increase the amount of scatter in our

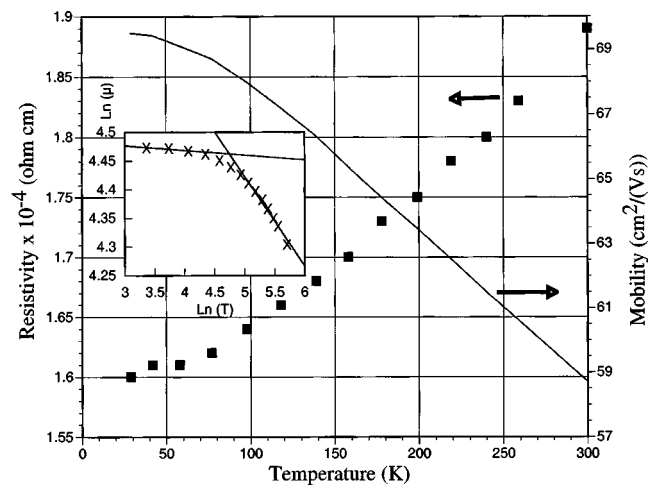


FIG. 5. Resistivity, mobility vs temperature for a typical cadmium stannate CTO film. Hall and resistivity data show film to be highly degenerate. Inset: $\ln(\text{mobility})$ vs $\ln(\text{temperature})$. The dominant scattering mechanism appears to change over the temperature range shown.

data. In hindsight, a Joule–Thomson refrigerator or an open-cycle helium or liquid nitrogen cryostat may have been a better choice.

Again, during the transverse Nernst voltage measurement, one must be careful of multiple transport phenomena occurring simultaneously. Note that because of the temperature gradient and the magnetic field, “hot” and “cold” diffusing carriers are deflected perpendicularly to the temperature gradient in the plane of the film. For an n -type material, when heater B is warmer than heater A and the magnetic field is in the z direction, contact 3 becomes warmer than contact 1. This phenomenon is known as the Righi–Leduc effect.¹⁵ The temperature difference will cause a Seebeck voltage to develop between contacts 3 and 1. Analogous to the interference of the Hall effect by the Ettingshausen effect, this unwanted voltage due to the Righi–Leduc effect is superimposed and inseparable from the Nernst voltage. However, the large thermal mass of the substrate and good thermal contact between the substrate and the heater blocks again minimize the unwanted effect. These conditions, and the fact that the natural temperature gradient of the cryostat is parallel to the short length of the sample, allow us to conclude that the temperature gradient between contacts 1

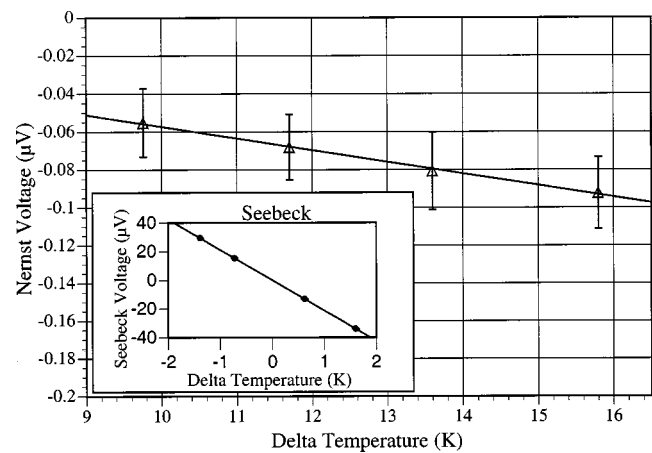


FIG. 6. Transverse Nernst voltage vs delta temperature. Data show a negative Nernst coefficient, indicative of an inverse relationship between relaxation time and carrier energy. Inset: Seebeck voltage vs delta temperature. Sign of slope indicates an n -type material, with a thermopower equal to the slope plus a system correction.

and 3 is negligible. To test this hypothesis, a type T differential thermocouple was mounted near contacts 1 and 3 and monitored during a Nernst measurement. No temperature difference was detected during this test. A simple zeroing of the Nernst offset voltage before the magnetic field is turned on is sufficient to cancel all relevant offset voltages.

V. DATA

We have collected transport data with our instrument on several transparent conductive oxide samples. We present, in this report, examples of our transport data on the CTO cadmium stannate, but wish to emphasize the far broader applicability to other semiconductors. Figure 5 shows mobility and resistivity versus temperature for a typical cadmium stannate film. The inset graph shows two distinct slopes in the plot of $\ln(\mu)$ vs $\ln(T)$, indicating a change in the dominant scattering mechanism near 100 K.¹⁸ The Hall data were nearly constant across this temperature range, illustrative of a degenerate semiconductor.

Figure 6 shows Seebeck and transverse Nernst voltages for a room-temperature cadmium stannate film with a Hall coefficient determined carrier concentration of $3.2 \times 10^{20} \text{ cm}^{-3}$. The Seebeck coefficient (slope of the line plus the system correction) is negative for this n -type mate-

TABLE I. Experimental and calculated values for a typical cadmium stannate CTO thin film. Calculated values were derived from solutions to the Boltzmann transport equation for a highly degenerate, parabolic band material.

	Thickness (μm)	Hall (m^3/C)	Resistivity ($\text{cm } \Omega$)	Seebeck ($\mu\text{V}/\text{K}$)	Nernst ($\mu\text{V}/\text{KT}$)
Measured value	0.17	$-1.98\text{E}-08$	$2.78\text{E}-04$	-19.20	$-2.37\text{E}-03$
Uncertainty	0.01	$8.9\text{E}-10$	$1.2\text{E}-05$	0.01	$2.6\text{E}-04$
	Mobility ($\text{cm}^2/\text{V s}$)	Carrier concentration (cm^{-3})	Fermi energy ^a (eV)	Effective mass (m/me)	Scattering parameter
Calculated value	71.2	$-3.15\text{E}+20$	0.57	0.30	-0.026
Uncertainty	4.4	$1.4\text{E}+19$	0.02	0.01	0.003

^aRelative to the conduction band.

rial. The Nernst data show the values of the transverse Nernst voltages at several different temperature gradients. These data were obtained by averaging the difference of the Nernst voltages measured with normal and reversed magnetic fields. The slope of the line gives $\Delta V_{1,3}/\Delta T_{2,3}$, which determines Q in the equation $Q = -(\Delta V_{1,3}d)/(\Delta T_{2,3}LB_z)$, where d , L , and B_z are defined in Figs. 1 and 2(b). The sign of the Nernst voltage reveals an inverse energy dependence on the relaxation time of the sample, indicative of phonon scattering in parabolic band, degenerate semiconductors.¹⁹

As previously mentioned in this report, we have established a method of calculating the effective mass, Fermi level, and energy-dependent scattering parameter of a film by measuring the four transport coefficients referred to above on a thin-film sample.²⁰ The density-of-states effective mass and the scattering parameter, s , associated with the relaxation-time approximation $\tau \propto E^s$, are determined from the equations:

$$m_d^* = \left(\frac{3n}{\pi}\right)^{2/3} \frac{q\hbar^2}{k_B^2 T} \left(\alpha - \frac{Q}{|R|\sigma}\right)$$

and

$$s = \frac{3}{2} \frac{(Q/|R|\sigma)}{(\alpha - Q/|R|\sigma)} + \lambda,$$

where $\lambda = (n/m_d^*)(dm_d^*/dn)$. λ is a measure of the nonparabolicity of the energy band and is zero for a parabolic energy band. The measured density-of-states effective mass for a series of samples with carrier concentrations from 2 to $7 \times 10^{20} \text{ cm}^{-3}$ was found to be approximately constant ($\lambda = 0$), with an average value of $0.29 \pm 0.04 m_e$. We conclude that cadmium stannate, in this range of carriers, has a nearly parabolic conduction band, which justifies our use of parabolic band theory in our calculations of E_f and s . Measured and calculated data for a typical cadmium stannate film are shown in Table I. The low value of s obtained from our CTO samples is most closely associated with a neutral impurity scattering mechanism ($s=0$), but is, perhaps, due to a variety of scattering mechanisms. The value for the effective mass is in good agreement with other work on this material where scattering mechanisms were assumed rather than measured,^{21,22} and with measured values first reported by Mulligan.²³

VI. DISCUSSION

The method of four coefficients is an ideal experimental technique for low-mobility thin films, as well as for high-

purity, single-crystal materials. The transport theory supporting the method is readily adaptable to nonparabolic energy band materials and is thus quite general. Our characterization of CdO and ZnO thin films by this method has substantiated their nonparabolic conduction energy bands predicted by theory and has shed new light on the type of scattering occurring in the films.

ACKNOWLEDGMENTS

The authors gratefully acknowledge the contributions of Dr. Philip A. Parilla, Dr. Timothy A. Gessert, Dr. Xuanzhi Wu, and W. Grover Coors to this work.

- ¹H. Mette, W. W. Gartner, and C. Loscoe, Phys. Rev. **115**, 537 (1959).
- ²H. Mette, W. W. Gartner, and C. Loscoe, Phys. Rev. **117**, 1491 (1960).
- ³V. I. Kaidanov and I. S. Lisker, Zavodskaya Laboratoriya **32**, 1091 (1966).
- ⁴V. I. Kaidanov and I. A. Chernik, Sov. Phys. Semicond. **1**, 1159 (1967).
- ⁵B. Y. Moizhes and Y. I. Ravich, Sov. Phys. Semicond. **1**, 149 (1967).
- ⁶I. A. Chernik, V. I. Kaidanov, N. V. Kolomets, and M. I. Vinogradova, Sov. Phys. Semicond. **2**, 645 (1968).
- ⁷W. Jiang, S. N. Mao, X. X. Xi, X. Jiang, J. L. Peng, T. Venkatesan, C. J. Lobb, and R. L. Greene, Phys. Rev. Lett. **73**, 1291 (1994).
- ⁸M. S. Balmaseda, J. C. G. d. Sande, and J. M. G. Perez, Phys. Rev. B **50**, 14561 (1994).
- ⁹G. Gordillo, B. Paez, C. Jacome, and J. M. Florez, Thin Solid Films **342**, 160 (1999).
- ¹⁰M. K. Zhitinskaya, V. I. Kaidanov, and I. A. Chernik, Sov. Phys. Solid State **8**, 295 (1966).
- ¹¹J. Kolodziejczak and S. Zukotynski, Phys. Status Solidi **5**, 145 (1964).
- ¹²W. Zawadzki and J. Kolodziejczak, Phys. Status Solidi **6**, 419 (1964).
- ¹³Annual Book of ASTM Standards (American Society of Testing and Materials, West Conshohocken, 1996).
- ¹⁴J. Yeager and M. A. Hrusch-Tupta, Low Level Measurements, Precision dc Current, Voltage and Resistance Measurements, 5th ed. (Keithley Instruments, Inc., Cleveland, 1997).
- ¹⁵E. Putley, The Hall Effect and Related Phenomena (Butterworths, London, 1960).
- ¹⁶R. B. Roberts, in Thermophysical Properties of Some Key Solids, edited by G. Y. White and M. L. Minges (Pergamon, Oxford, 1985).
- ¹⁷C. Y. Ho, Purdue University-Center for Information and Numerical Data Analysis and Synthesis, West Lafayette, 1989.
- ¹⁸S. S. Li, Semiconductor Physical Electronics (Plenum, New York, 1993).
- ¹⁹B. M. Askerov, Electron Transport Phenomena in Semiconductors (World Scientific, Singapore, 1994).
- ²⁰D. L. Young, T. J. Coutts, V. I. Kaydanov, and W. P. Mulligan, presented at the 46th International Symposium of the American Vacuum Society, 1999 (unpublished).
- ²¹E. Leja, T. Stapinski, and K. Marszalek, Thin Solid Films **125**, 119 (1985).
- ²²T. Pisarkiewicz, K. Zakrzewska, and E. Leja, Thin Solid Films **153**, 479 (1987).
- ²³W. P. Mulligan, Ph.D. thesis, Colorado School of Mines, 1997.